Thermodynamic signatures for topological phase transitions to Majorana and Weyl superfluids in ultracold Fermi gases

Kangjun Seo,[1] Chuanwei Zhang,[2] and Sumanta Tewari[1]
[1]*Department of Physics and Astronomy, Clemson University, Clemson, South Carolina 29634, USA*
[2]*Department of Physics, The University of Texas at Dallas, Richardson, Texas 75080 USA*
(Received 8 April 2013; published 19 June 2013)

We discuss the thermodynamic signatures for the topological phase transitions into Majorana and Weyl superfluid phases in ultracold Fermi gases in two and three dimensions (2D and 3D) in the presence of Rashba spin-orbit coupling and a Zeeman field. We analyze the thermodynamic properties exhibiting the distinct nature of the topological phase transitions linked with the Majorana fermions (2D Fermi gas) and Weyl fermions (3D Fermi gas) which can be observed experimentally, including pressure, chemical potential, isothermal compressibility, entropy, and specific heat, as a function of the interaction and the Zeeman field at both zero and finite temperatures. We conclude that among the various thermodynamic quantities, the isothermal compressibility and the chemical potential as functions of the artificial Zeeman field have the strongest signatures of the topological transitions in both two and three dimensions.

DOI: 10.1103/PhysRevA.87.063618 PACS number(s): 03.75.Ss, 67.85.Lm

I. INTRODUCTION

Ultracold fermionic quantum gases have many advantages in the investigation of quantum phenomena in a highly tunable way. The experimental ability to control the interaction between the Fermi atoms via Feshbach resonances [1] enables one to study the crossover phenomena [2] from the BCS superfluid of weakly bound Cooper pairs to the Bose-Einstein condensate (BEC) of tightly bound molecules [3], universal properties in the unitary regime [4], vortices [5], and so forth. In addition, the experimental control of the internal spin states via radio frequencies provides the study of the emergence of new superfluid phases in a Fermi gas with population imbalance which serves as an effective Zeeman field [6–8]. Another new development enables one to trap two-dimensional (2D) fermions in the quantum degenerate regime [9,10].

Furthermore, in recent experimental breakthroughs spin-orbit coupling (SOC) has been developed using two-photon Raman processes in bosonic as well as fermionic gases [11–15], which has given rise to theoretical investigations of the new quantum states of matter [16–19]. Thus far, the experimental realization of SOC is an equal combination of Rashba [20] and Dresselhaus [21] types of SOC. It has been shown theoretically that in the presence of Rashba SOC and a perpendicular Zeeman field, 2D cold fermion systems with an s-wave Feshbach resonance can enter into a topological superfluid phase with zero-energy Majorana fermion excitations localized at the order parameter defects such as vortices [18,22,23]. It has also been shown that in three dimensions (3D) the corresponding system is capable of supporting the intriguing Weyl fermion excitations [17]. The realization of ultracold fermionic gases with Rashba SOC and a Zeeman field thus offers the tantalizing possibility of experimentally engineering all three kinds of fundamental relativistic fermions, namely, the Dirac, Weyl, and Majorana fermions [24]. In addition to these powerful experimental and theoretical developments, there have been more recently added to the list. One is the development of methods for high-precision measurements of the thermodynamic properties such as compressibility, chemical potential, entropy, and heat capacity for uniform s-wave Fermi superfluids [25,26]. In recent developments, Ref. [26] has completely determined the universal thermodynamics of an interacting Fermi gas across an s-wave superfluid transition and has captured the onset of superfluidity in the compressibility, chemical potential, entropy, and heat capacity.

The question we address in this paper is what are the corresponding thermodynamic signatures for interacting ultracold fermions across the *topological* superfluid transitions to phases supporting Majorana fermions (2D) and Weyl fermions (3D). Our main conclusion is that among the various thermodynamic quantities, the isothermal compressibility and the chemical potential as functions of the artificial Zeeman field have the strongest signatures of the topological transitions. The signatures for the transition from the nontopological s-wave superfluid to the Majorana superfluid phase in 2D are stronger than the corresponding signatures in 3D where the transition is in the Weyl superfluid phase. The other thermodynamic quantities such as pressure, entropy, and specific heat have only weak signatures of the topological transitions (that is, the transition between a nontopological superfluid and a topological superfluid as a function of the Zeeman field), even though they are useful in capturing the topological superfluid to the normal phase (pair potential $\Delta = 0$) transitions in both two and three dimensions.

In condensed matter systems, SOC, which results from the coupling between the spin degrees of freedom and the orbital motion of a quantum particle, plays an important role in understanding interesting physics associated with the topological quantum phenomena including the spin Hall effect [27,28], topological insulators [29], and topological superconductors [30]. These phases generically arise as a result of topological quantum phase transitions (TQPT) in the appropriate systems. TQPTs separate distinct phases of matter which have exactly the same symmetries and thus

are not associated with any spontaneous symmetry breaking in the underlying Hamiltonian. Yet, the phases separated by TQPTs have distinct topological properties which can often manifest themselves in the properties of the order parameter defects. For instance, it has been pointed out recently that spin-orbit-coupled electron- or hole-doped semiconductor thin films (2D) or nanowires (1D) with proximity-induced s-wave superconductivity and a suitably directed Zeeman field (Γ) support novel non-Abelian topological states with the order parameter defects supporting localized topological zero-energy excitations called Majorana fermions [31–36] above a critical Zeeman field ($\Gamma > \Gamma_c$). These theoretical developments in the condensed matter system followed earlier similar proposals in the context of ultracold fermions in two dimensions in the presence of artificial SOC and a Zeeman field and with s-wave pairing interactions [22]. While the two-dimensional cold fermion systems support the Majorana fermions in the order parameter defects (but are otherwise completely gapped in the bulk), the corresponding three-dimensional systems have topologically protected gapless nodes in the bulk supporting the relativistic Weyl fermion excitations. With Rashba-type of SOC and an increasing strength of the Zeeman field, the three-dimensional system supports a series of 3D topological quantum phase transitions [37] from a nontopological superfluid state with fully gapped fermionic excitations to a topological superfluid state with four protected Fermi points (i.e., gap nodes) and then to a second topological superfluid state with only two protected Fermi points [17]. Such 3D topological gapless superfluids with Weyl fermions, which result from quasiparticle excitations in a linearized Hamiltonian near the nodes, are different from the 2D fully gapped topological superfluids with Majorana fermions [18,31]. Recently, similar Weyl fermion physics in an analogous 3D condensed matter system has also been discussed in the context of ferromagnetic superconductors [38]. The results of the thermodynamic signatures of the topological transitions to Majorana and Weyl superfluid phases discussed in this paper apply to both cold fermion and condensed matter systems, although our focus will mostly be ultracold fermions where the methods for high-precision measurements of the thermodynamic quantities have recently been successfully developed.

The paper is organized as follows. In Sec. II, we derive the mean-field order parameter and atom-number equations for ultracold fermions with Rashba SOC and a Zeeman field. We present in Sec. III the zero-temperature phase diagram and the thermodynamic quantities as functions of the interaction for both 2D and 3D Fermi superfluids from the self-consistent numerical calculations. Section IV provides the phase diagram and corresponding thermodynamic properties at finite temperature. Section V consists of discussion and conclusions.

II. MEAN-FIELD THEORY

The system we consider is a uniform s-wave fermionic superfluid with the atom density $n = N/V$ in the presence of Rashba-type spin-orbit coupling in the xy plane and a Zeeman field along the z direction. The dynamics of the Fermi gas can be described by the Hamiltonian $H = H_0 + H_{\rm int}$, where the single-particle Hamiltonian

$$H_0 = \sum_{\gamma\gamma'} \int d\mathbf{r} c^\dagger_{\mathbf{r}\gamma} \left[\xi(\mathbf{r}) I - i\hbar\alpha\left(\partial_y\sigma_x - \partial_x\sigma_y\right) + \Gamma\sigma_z\right]_{\gamma\gamma'} c_{\mathbf{r}\gamma'}, \tag{1}$$

where $\gamma = \uparrow,\downarrow$ are the pseudospins of the atoms, $\xi(\mathbf{r}) = -\hbar^2\nabla^2/2m - \mu$, μ is the chemical potential, α is the Rashba SOC strength, I is the 2×2 unit matrix, σ_i is the Pauli matrix, Γ is the strength of the Zeeman field, and $c_{\mathbf{r}\gamma}$ is the atom annihilation operator. $H_{\rm int} = -g\int d\mathbf{r}\, c^\dagger_{\mathbf{r}\uparrow} c^\dagger_{\mathbf{r}\downarrow} c_{\mathbf{r}\downarrow} c_{\mathbf{r}\uparrow}$ is the s-wave scattering interaction with $g = 4\pi\hbar^2\bar{a}_s/m$, and the scattering length $\bar{a}_s$ can be tuned by the Feshbach resonance.

The grand partition function at temperature T is $Z = \int D[\psi,\bar{\psi}]\exp(-S[\psi,\bar{\psi}])$ with action

$$S[\psi,\bar{\psi}] = \int_0^{1/T} d\tau \left[\sum_\gamma \int d\mathbf{r}\bar{\psi}_\gamma(x)\partial_\tau\psi_\gamma(x) + \mathcal{H}[\psi,\bar{\psi}]\right], \tag{2}$$

where $x = (\mathbf{r},\tau)$ and $\mathcal{H}[\psi,\bar{\psi}]$ is the many-body Hamiltonian with field operators $c_{\mathbf{r}\gamma}$ and $c^\dagger_{\mathbf{r}\gamma}$ replaced by the anticommuting c-numbers, Grassmann variables, $\psi_\gamma(x)$ and $\bar{\psi}_\gamma(x)$, respectively. Using the standard Hubbard-Stratonovich transformation that introduces the pairing potential $\Delta(x) = g\langle\psi_\downarrow(x)\psi_\uparrow(x)\rangle$ and integrating over the fermion variables lead to the effective action

$$S_{\rm eff}[\Delta,\bar{\Delta}] = \int d\tau d\mathbf{r}\left[\frac{|\Delta(x)|^2}{g} - \frac{T}{2V}\ln\det\frac{\mathbf{M}}{T} + \xi(\mathbf{r})\right], \tag{3}$$

where the matrix $\mathbf{M}$ is

$$\mathbf{M} = \begin{pmatrix} \partial_\tau - \xi_\uparrow(\mathbf{r}) & -h_\perp(\mathbf{r}) & 0 & \Delta(x) \\ h^*_\perp(\mathbf{r}) & \partial_\tau - \xi_\downarrow(\mathbf{r}) & -\Delta(x) & 0 \\ 0 & -\bar{\Delta}(x) & \partial_\tau + \xi_\uparrow(\mathbf{r}) & h^*_\perp(\mathbf{r}) \\ \bar{\Delta}(x) & 0 & -h_\perp(\mathbf{r}) & \partial_\tau + \xi_\downarrow(\mathbf{r}) \end{pmatrix}, \tag{4}$$

where $h_\perp(\mathbf{r}) = -i\hbar\alpha(\partial_y + i\partial_x)$ corresponds to the transverse component of the SOC field, Γ to the parallel component with respect to the quantization axis z, and $\xi_{\uparrow,\downarrow}(\mathbf{r}) = \xi(\mathbf{r}) \pm \Gamma$.

To proceed, we use the saddle-point approximation $\Delta(x) = \Delta + \Delta_F(x)$, and write $\mathbf{M} = \mathbf{M}_0 + \mathbf{M}_F$. The matrix $\mathbf{M}_0$ is obtained via the saddle point $\Delta(x) \to \Delta$ which takes $\mathbf{M} \to \mathbf{M}_0$, and the functional matrix $\mathbf{M}_F = \mathbf{M} - \mathbf{M}_0$ depends only on $\Delta_F(x)$ and its Hermitian conjugate. Thus, we write the effective action as $S_{\rm eff} = S_0 + S_F$. The first term is

$$S_0[\Delta,\Delta^*] = \frac{V}{T}\frac{|\Delta|^2}{g} - \frac{1}{2}\sum_{\mathbf{k},i\omega_n,\eta,\lambda}\ln\left(\frac{i\omega_n - E^\lambda_{\mathbf{k},\eta}}{T}\right) + \sum_{\mathbf{k}}\frac{\xi_{\mathbf{k}}}{T}, \tag{5}$$

where $\omega_n = (2n+1)\pi T$ and $\xi_{\mathbf{k}} = \mathbf{k}^2/2m - \mu$. Here $E^\lambda_{\mathbf{k},\eta}$ are the eigenvalues of

$$\mathbf{M}_{\mathbf{k}} = \begin{pmatrix} \xi_{\mathbf{k}} + \Gamma & h_\perp(\mathbf{k}) & 0 & -\Delta \\ h^*_\perp(\mathbf{k}) & \xi_{\mathbf{k}} - \Gamma & \Delta & 0 \\ 0 & \Delta^* & -\xi_{\mathbf{k}} - \Gamma & h^*_\perp(\mathbf{k}) \\ -\Delta^* & 0 & h_\perp(\mathbf{k}) & -\xi_{\mathbf{k}} + \Gamma \end{pmatrix}, \tag{6}$$

which describes the Hamiltonian of elementary excitations in the four-component Nambu spinor $\Psi_{\mathbf{k}} = (c_{\mathbf{k}\uparrow}, c_{\mathbf{k}\downarrow}, c^{\dagger}_{-\mathbf{k}\uparrow}, c^{\dagger}_{-\mathbf{k}\downarrow})^{\dagger}$. Here, $h_{\perp}(\mathbf{k}) = \alpha(k_y + ik_x)$, and the quasiparticle excitation energy

$$E^{\lambda}_{\mathbf{k}\pm} = \lambda\sqrt{\xi^2_{\mathbf{k}} + \alpha^2 k^2_{\perp} + \Gamma^2 + |\Delta|^2 \pm 2E_0} \tag{7}$$

is the eigenvalue of $M_{\mathbf{k}}$, where $\lambda = \pm$ correspond to the particle and hole branches, $E_0 = \sqrt{\Gamma^2(\xi^2_{\mathbf{k}} + |\Delta|^2) + \alpha^2 k^2_{\perp}\xi^2_{\mathbf{k}}}$, and $k_{\perp} = \sqrt{k^2_x + k^2_y}$. For $\alpha = \Gamma = 0$, Eq. (7) reduces to $E^{\lambda}_{\mathbf{k}} = \lambda\sqrt{\xi^2_{\mathbf{k}} + |\Delta|^2}$ in the standard BCS theory.

The saddle-point grand potential function $\Omega = -T \ln Z_0$ is

$$\Omega = V\frac{|\Delta|^2}{g} - \frac{T}{2}\sum_{\mathbf{k},\eta,\lambda} \ln(1 + e^{-E^{\lambda}_{\mathbf{k},\eta}/T}) + \sum_{\mathbf{k}} \xi_{\mathbf{k}}, \tag{8}$$

leading to the order parameter via minimization of Ω with respect to Δ:

$$\frac{\Delta}{g} + \frac{1}{2V}\sum_{\mathbf{k},\eta,\lambda} f(E^{\lambda}_{\mathbf{k},\eta})\left(\frac{\partial E^{\lambda}_{\mathbf{k},\eta}}{\partial \Delta^*}\right) = 0, \tag{9}$$

where $f(x) = 1/[1 + \exp(-x/T)]$ is the Fermi-Dirac distribution function. For the case of 2D gas, Eq. (9) can be expressed as

$$\sum_{\mathbf{k},\eta}\left[(1 - \eta\Gamma^2/E_0)\tanh(E^{+}_{\mathbf{k},\eta}/2T)/4E^{+}_{\mathbf{k},\eta} - \frac{1}{2\epsilon_{\mathbf{k}} + E_b}\right] = 0,$$

where $E_b = \hbar^2/ma^2$ is the binding energy controlled by Feshbach resonances; and for 3D gas,

$$\frac{Vm}{4\pi\hbar^2 a_s} = -\sum_{\mathbf{k},\eta}\left[(1 - \eta\Gamma^2/E_0)\tanh(E^{+}_{\mathbf{k},\eta}/2T)/4E^{+}_{\mathbf{k},\eta} - \frac{1}{2\epsilon_{\mathbf{k}}}\right].$$

The ultraviolet divergence at the large $\mathbf{k}$ in Eq. (9) has been regularized by subtracting the term $1/2\epsilon_{\mathbf{k}}$, and a_s is defined as the renormalized scattering length. The total number of atoms can be obtained from $N = -(\partial\Omega/\partial\mu)$:

$$N = \sum_{\mathbf{k},\eta}\left[1 + \left(\frac{\eta(\alpha^2 k^2_{\perp} + \Gamma^2)}{E_0} - 1\right)\frac{\xi_{\mathbf{k}}}{2E^{+}_{\mathbf{k},\eta}}\tanh(E^{+}_{\mathbf{k},\eta}/2T)\right]. \tag{10}$$

We self-consistently solve the order parameter equation (9) and the number equation (10) for different parameters $(\alpha K_F, \Gamma, \nu, T)$ for a fixed atom density n to determine Δ and μ. Here $\nu = 1/K_F a_s$, and $K_F = (3\pi^2 n)^{1/3}$ is the Fermi momentum for a noninteracting 3D Fermi gas with the same density at $\Gamma = \alpha = 0$ and $\nu = E_b$ and $K_F = (2\pi n)^{1/2}$ for a noninteracting 2D Fermi gas. The energy unit is chosen as the Fermi energy $E_F = \hbar^2 K^2_F/2m$.

III. TOPOLOGICAL PHASE TRANSITIONS DURING BCS-BEC CROSSOVER ($T = 0$)

A. Phase diagram

In Fig. 1, we show the mean-field zero-temperature phase diagram as a function of the Zeeman field Γ and the interaction parameter ν in the presence of Rashba SOC ($\alpha K_F = 0.4$). We label the uniform topologically nontrivial s-wave superfluid phases with zero, one, two, and four nodal points as TS_0, TS_1, TS_2, and TS_4, respectively. For a 2D Fermi gas as in Fig. 1(a), a topologically nontrivial superfluid phase with one node, TS_1, occurs only along the $\Gamma = \Gamma_c = \sqrt{\mu^2 + \Delta^2}$ line. Even though below and above $\Gamma = \Gamma_c$, the superfluid gap remains finite everywhere in the momentum space, thus the excitation spectrum is fully gapped, Γ_c is a phase boundary between the nontopological superfluid (NTS) and nontrivial (TS_0) superfluid phases. Even though the TS_0 phase is fully gapped, the phase is topologically nontrivial because in the presence of an order parameter defect such as a vortex, the vortex core supports a nondegenerate zero-energy Majorana fermion excitation. The TS_0 phase has recently received wide attention in condensed matter physics [31–36,39–41] where 2D semiconducting thin films and 1D semiconducting nanowires with proximity induced s-wave superconductivity and a Zeeman field have been shown to support Majorana fermions in order parameter defects such as vortices and boundaries. Such localized Majorana fermion excitations are thought to support non-Abelian statistics, which has been proposed as a key resource for fault-tolerant topological quantum computation (TQC) [42]. The 2D ultracold fermionic gases with laser-induced Rashba SOC and a Zeeman field in the TS_0 phase can also support Majorana fermions in vortices and sample boundaries and thus can potentially act as a platform for fault-tolerant TQC. In contrast, for a 3D Fermi superfluid as in Fig. 1(b), the blue dot-dashed line determined by the Chandrasekhar-Clogston-like condition $\Gamma = \Delta$ is a topological phase boundary between fully gapped NTS ($\Gamma < \Delta$) and gapless TS ($\Gamma > \Delta$) phases. In addition, within the gapless TS phase, Γ_c is a quantum critical point of the topological phase transition between the TS phases with two (TS_2) and four (TS_4) nodes. The fermions with linear

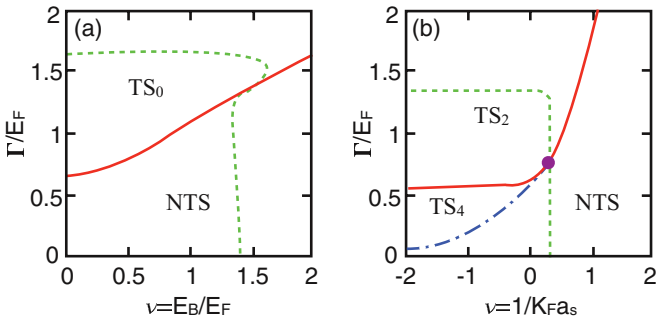

FIG. 1. (Color online) $(\Gamma - \nu)$ phase diagram for (a) 2D and (b) 3D Fermi gases at $T = 0$ with $\alpha K_F = 0.4$. Here, ν represents interaction parameters, E_B/E_F for 2D and $1/K_F a_s$ for 3D systems. We label the fully gapped nontopological superfluid phase as NTS, fully gapped topological superfluid phase as TS_0, and topological superfluids with two and four nodes as TS_2 and TS_4, respectively. Red solid and blue dot-dashed lines denote $\Gamma_c = \sqrt{\mu^2 + \Delta^2}$ and $\Gamma_{\Delta} = \Delta$, respectively, where the topological phase transitions occur. Green dashed lines correspond to $\mu = 0$, below which $\mu > 0$ and above which $\mu < 0$. Note that TS_4 superfluid phase, which is characterized by 4 nodes along z-axis, arises when $\mu > 0$ and merges at the tricritical point, which is indicated by purple circle in the phase diagram of 3D fermion superfluid.

dispersion relations near each node in the TS_2 and TS_4 phases are manifestations of the relativistic Weyl fermions. The bulk nodal excitation spectra of these phases are also topologically protected and a topological invariant characterizing the nodal points (in the context of He-3) was formulated by Volovik [37]. Recently, similar topologically protected Weyl fermion modes have been shown to exist also in condensed matter systems such as ferromagnetic superconductors [38].

B. Chemical potential

Chemical potential can be calculated by solving the order parameter equation with the total number of the system fixed self-consistently. With Zeeman field Γ and interaction ν as tuning parameters, one can have chemical potential as a function of Γ and ν, that is, $\mu = \mu(\Gamma, \nu)$.

In Fig. 2, we show the chemical potential as a function of Γ for a given interaction ν and SOC αK_F. Figures 2(a) and 2(b) are plots of the chemical potential μ and its derivative with respect to Γ, $\frac{d\mu}{d\Gamma}$, for 2D Fermi gas at $E_b = 0.5E_F$ and $\alpha K_F = 0.4$. In the side of a low Zeeman field Γ, where $\Gamma < \Gamma_c = \sqrt{\mu^2 + \Delta^2}$ and the system is in the nontopological superfluid phase (NTS), μ is slowly varying as Γ increases. In the region of a strong Zeeman field, where $\Gamma > \Gamma_c$ and the system is in a gapped TS_0 phase, μ decreases fast with increasing Γ. Near the quantum critical point Γ_c, the slope changes discontinuously as can be seen clearly in the plot of $\frac{d\mu}{d\Gamma}$ in Fig. 2(b), indicating the change in the curvature.

As for the 3D Fermi superfluids, topological phase transition from a fully gapped NTS to a gapless TS_4 state occurs at Zeeman field $\Gamma = \Gamma_\Delta = \Delta$, and the TS_4 to TS_2 phase transition occurs at $\Gamma = \Gamma_c = \sqrt{\mu^2 + \Delta^2}$. Figures 2(c) and 2(d) illustrate μ as a function of Γ at unitarity ($1/K_F a_s = 0$) with the same SOC strength as that in 2D fermion gases. Even though the signatures of topological phase transitions across the phase boundaries are weaker than the one for the 2D Fermi system, μ in the fully gapped NTS phase ($\Gamma < \Gamma_\Delta$) increases with increasing Γ, while μ decreases with increasing Γ when it is in the TS_2 phase ($\Gamma > \Gamma_c$). The curvature of the chemical potential versus the Zeeman field changes as the system moves from the gapped to the gapless phases and vice versa. In contrast to the 2D Fermi superfluid, however, the $\frac{d\mu}{d\Gamma}$ plot does not exhibit a cusp at the phase boundary because of the existence of the TS_4 phase surrounded by the gapped NTS and gapless TS_2 phases. It is when $\mu = 0$ that the two distinct critical points Γ_Δ and Γ_c merge ($\Gamma_\Delta = \Gamma_c$) and a tricritical point occurs, leading to the vanishing of the TS_4 phase and the emergence of the cusp in $\frac{d\mu}{d\Gamma}$ even in a 3D Fermi superfluid system.

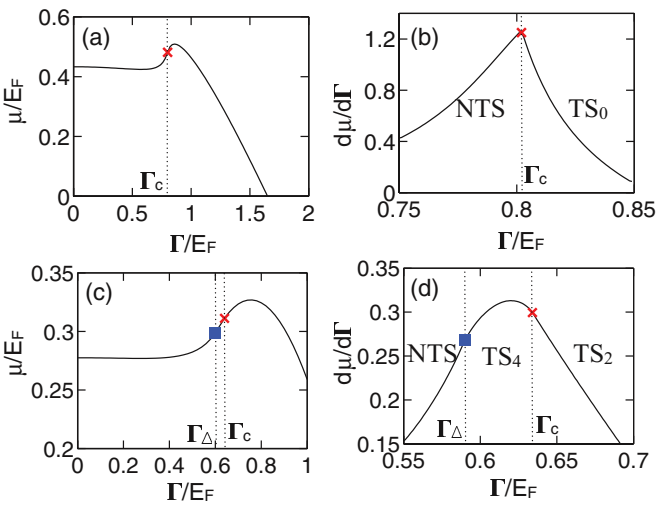

FIG. 2. (Color online) Chemical potential μ and its derivative with respect to Γ, $\frac{d\mu}{d\Gamma}$ for (a), (b) 2D Fermi gas at $E_b = 0.5E_F$ and (c), (d) 3D Fermi gas at $1/K_F a_s = 0$ with $\alpha K_F = 0.4$. Red cross and blue square indicate the critical points $\Gamma_\Delta = \Delta$ and $\Gamma_c = \sqrt{\mu^2 + \Delta^2}$, respectively. One finds that a fully gapped NTS phase occurs at $\Gamma < \Gamma_c$ for 2D and $\Gamma < \Gamma_\Delta$ for 3D gases.

C. Compressibility

The compressibility can be obtained from the knowledge of the pressure, as defined by $\kappa_T = -(1/V)(\partial p/\partial V)$. But in the grand-canonical ensemble, where we need to fix the average number of particles, the isothermal compressibility can be directly written as

$$\kappa_T = \frac{1}{N^2}\left(\frac{\partial N}{\partial \mu}\right)_{T,V}. \tag{11}$$

In the superfluid state, we need to consider μ dependence of Δ. From the order parameter equation $(\partial\Omega/\partial\Delta) = 0$, we have $(\partial/\partial\mu)(\partial\Omega/\partial\Delta) = 0$, leading to

$$\left(\frac{\partial\Delta}{\partial\mu}\right)_{T,V} = -\left(\frac{\partial N}{\partial\Delta}\right)_{T,V,\mu}\left(\frac{\partial^2\Omega}{\partial\Delta^2}\right)^{-1}_{T,V,\mu}. \tag{12}$$

Thus the isothermal compressibility in the superfluid phase can be written as

$$\kappa_T = \frac{1}{N^2}\left[\left(\frac{\partial N}{\partial\mu}\right)_{T,V,\Delta} - \left(\frac{\partial N}{\partial\Delta}\right)^2_{T,V,\mu}\left(\frac{\partial^2\Omega}{\partial\Delta^2}\right)^{-1}_{T,V,\mu}\right]. \tag{13}$$

In Fig. 3, we present the isothermal compressibility κ_T as a function of Γ for a given interaction ν at $T = 0$ with $\alpha K_F = 0.4$ to investigate the signature of the topological phase transitions. Since κ_T is related to the first derivative of the total number N with respect to μ, that is, $\kappa_T \sim \frac{\partial N}{\partial\mu}|_{T,V}$, it is expected to show the signatures of the topological phase transitions as seen in the plots of μ in Fig. 2. In Fig. 3, κ_T shows a decreasing trend in the superfluid phase with increasing Γ, while it is an

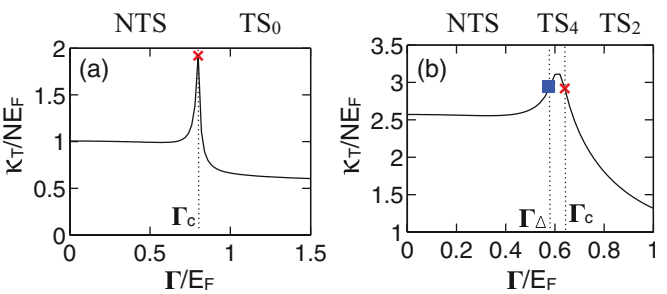

FIG. 3. (Color online) Isothermal compressibility κ_T as a function of Γ for (a) 2D Fermi gas at $E_b = 0.5E_F$ and (b) 3D Fermi gas at $1/K_F a_s = 0$ with $\alpha K_F = 0.4$. Red cross and blue square indicate the critical points $\Gamma_\Delta = \Delta$ and $\Gamma_c = \sqrt{\mu^2 + \Delta^2}$, respectively, same as in Figs. 1 and 2.

increasing function of Γ in normal phase as will be shown in Fig. 5. For 2D uniform Fermi superfluids, at the critical Zeeman field Γ_c, a sharp peak emerges as shown in Fig. 3(a). This peak in the compressibility corresponds to the phase boundary between the 2D gapped NTS and the 2D gapped TS_0 phases. In our calculations we find that the compressibility provides the strongest signature of the phase transition to the 2D topological phase with the Majorana fermion excitations. In 2D at zero temperature there is no additional phase transition from the TS_0 phase to the normal phase at higher values of Γ. This is because, with a finite Rashba SOC, the superfluid pair potential always remains nonzero even at large values of the Zeeman field. When the temperature is included as another parameter on the phase diagram, a normal phase with $\Delta = 0$ emerges even in 2D (see below).

As for the 3D case, Fig. 3(b) shows that $\kappa_T(\Gamma)$ again decreases with increasing Γ in the superfluid phase, and shows the signature of the topological phase transitions by a smoothly peaked curve near $\Gamma = \Gamma_c$. As already seen in the plot of μ vs Γ, κ_T of the 3D fermion system in the TS_4 phase, which is sandwiched between the gapped NTS and gapless TS_2 phases, is a fast varying function of Γ, while the compressibility in the gapped NTS phase is slowly varying.

IV. THERMODYNAMIC SIGNATURES ($T \neq 0$)

Experimentally, the thermodynamic properties of a given substance are determined by measuring an equation of state (EOS), such as the pressure $p(\mu,T)$ as a function of the chemical potential μ and the temperature T. Equivalently, replacing the pressure by the density $n = (\frac{\partial p}{\partial \mu})_T$, one can determine the density EOS, $n(\mu,T)$. The local gas density $n(V)$ can be measured [26] as a function of the local trapping potential V from *in situ* absorption images of a trapped, strongly interacting Fermi gas at a Feshbach resonance. From the definition of the compressibility $\kappa_T = \frac{1}{N^2}(\frac{\partial N}{\partial \mu})_T$, the chemical potential as a function of temperature T is attainable experimentally without numerical derivatives of the data [26]. Then, from the energy, pressure, and chemical potential, entropy $S = \frac{1}{T}(E + pV - \mu N)$ and specific heat c_V can be obtained as functions of temperature T.

A. Thermodynamic properties

From the mean-field grand partition function

$$Z = \mathrm{Tr}(e^{-(H-\mu N)/T}), \tag{14}$$

we can calculate the corresponding grand potential function $\Omega = -T \ln Z = \langle H \rangle - TS - \mu \langle N \rangle = -pV$, where S is the entropy and p is the pressure of the system. The differential of the grand potential function is

$$d\Omega = -S\,dT - p\,dV - \langle N \rangle\, d\mu, \tag{15}$$

allowing us to obtain interesting thermodynamic properties. The explicit expression of Ω in terms of the Hamiltonian under consideration is

$$\Omega = -\frac{T}{2}\sum_{\mathbf{k},\eta,\lambda} \ln\left(1 + e^{-E^{\lambda}_{\mathbf{k},\eta}/T}\right) + \sum_{\mathbf{k}} \xi_{\mathbf{k}} + V\frac{|\Delta|^2}{g}. \tag{16}$$

Then, the pressure of the ultracold Fermi gas can be obtained through the grand potential function via $p = -\Omega/V$. In the thermodynamic limit, it reads

$$p = -\frac{T}{2}\sum_{\eta,\lambda}\int \frac{d^Dk}{(2\pi)^D} \ln\left(1 + e^{-E^{\lambda}_{\mathbf{k},\eta}/T}\right) + \int \frac{d^Dk}{(2\pi)^D}\xi_{\mathbf{k}} + \frac{|\Delta|^2}{g}. \tag{17}$$

The entropy can be obtained by

$$S = -\left(\frac{\partial \Omega}{\partial T}\right)_{\mu,V}. \tag{18}$$

Then, the heat capacity can be obtained from the knowledge of the entropy:

$$c_V = \left(\frac{\partial S}{\partial T}\right)_{\mu,V}. \tag{19}$$

In the superfluid phase, Δ depends on temperature T as

$$\left(\frac{\partial \Delta}{\partial T}\right)_{\mu,V} = -\left(\frac{\partial S}{\partial \Delta}\right)_{T,V,\mu}\left(\frac{\partial^2 \Omega}{\partial \Delta^2}\right)^{-1}_{T,V,\mu}, \tag{20}$$

leading to the specific heat in the superfluid phase

$$c_V = \left(\frac{\partial S}{\partial T}\right)_{\mu,V,\Delta} - \left(\frac{\partial S}{\partial \Delta}\right)^2_{T,V,\mu}\left(\frac{\partial^2 \Omega}{\partial \Delta^2}\right)^{-1}_{T,V,\mu}. \tag{21}$$

B. Finite-temperature phase diagram

Figure 4 presents mean-field ($T - \Gamma$) phase diagrams for 2D and 3D homogeneous Fermi gases in the presence of Rashba type of spin-orbit coupling. We choose the interaction parameter ν as a two-body binding energy $E_b = 0.5E_F$ forthe 2D Fermi gas [Fig. 4(a)], while $1/K_F a_s = 0$ for the 3D Fermi gas [Fig. 4(b)] with Rashba SOC $\alpha K_F = 0.4$. With increasing temperature T, the superfluid order parameter Δ decreases and undergoes the second-order phase transition to normal phase ($\Delta = 0$) denoted as N at $T = T_c$.

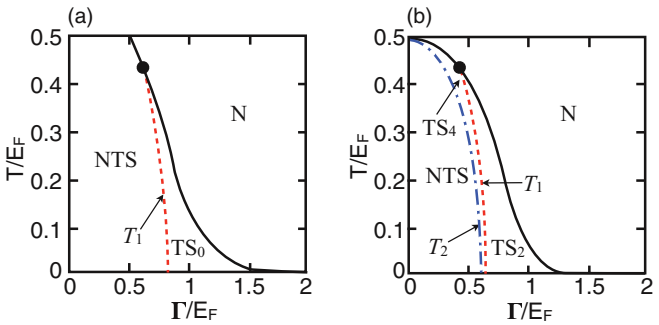

FIG. 4. (Color online) ($\Gamma - T$) phase diagrams for (a) 2D Fermi gas at $E_b = 0.5E_F$ and (b) 3D Fermi gas $1/K_F a_s = 0$ with $\alpha K_F = 0.4$. Red dashed and blue dot-dashed lines denote $\Gamma_c = \sqrt{\mu^2 + \Delta^2}$ and $\Gamma_\Delta = \Delta$, respectively. Black solid lines represent Γ_0 above which the order parameter vanishes, or $\Delta = 0$. The tricritical temperatures, at which Γ_c meets with Γ_0 (black circles), for 2D and 3D gases are $T = 0.43E_F$ at $\Gamma_c = \Gamma_0 = 0.62E_F$ and $T = 0.44E_F$ at $\Gamma_c = \Gamma_0 = 0.42E_F$,respectively.

In Fig. 4(a), within the superfluid phase of the 2D fermion gas, topological phase transition between the gapped NTS phase ($\Gamma < \Gamma_c$) and the gapped TS_0 phase ($\Gamma > \Gamma_c$) occurs at $T = T_1 < T_c$ indicated with a red dashed line. In addition, the TS_0 phase vanishes at the tricritical temperature $T_1 = T_c = 0.43E_F$ with our choice of parameters E_b and α. In Fig. 4(b), T_2 (blue dot-dashed line) determined by the Chandrasekhar-Clogston-like condition, $\Gamma = \Delta$, is a phase boundary between the NTS phase ($T < T_2$) and the TS_4 phase ($T_2 < T < \min[T_c, T_1]$). It is when $\Gamma = 0$ that $T_2 = T_c$ occurs and the system above T_c becomes the normal state ($\Delta = 0$). Thus, for $\Gamma = 0$, there is only one finite-temperature phase transition at $T_c(=T_2)$ which is a transition between the nontopological superfluid (NTS) ($T < T_c$) and the normal state ($T > T_c$). In a similar manner as in the 2D system, the TS_4 phase vanishes at finite Γ, where $T_c = T_1 = 0.43E_F$ at unitarity ($1/K_F a_s = 0$).

C. Thermodynamic quantities as a function of temperature

Since we learned that the chemical potential and the isothermal compressibility at zero temperature can show the evidence of the topological phase transitions as a function of the tuning parameters such as the Zeeman field Γ and the interaction parameter ν, we first consider below the chemical potential and the compressibility at finite temperatures.

In Fig. 5, we show the chemical potential and isothermal compressibility as functions of the reduced Zeeman field Γ/Γ_0 for 2D on the left column and 3D on the right column at both $T > T_1$ (dashed) and $T < T_1$ (solid). We choose the Rashba SOC $\alpha K_F = 0.4$ and the interaction parameters $E_b = 0.5E_F$ for 2D and $1/K_F a_s = 0$ for 3D Fermi gases, respectively. Figures 5(a) and 5(b) show that, at low temperatures, $T < T_1$, κ_T for both 2D and 3D fermions exhibit peaks at or near the topological critical points, and a discontinuity at the phase transition to the normal state at $\Gamma = \Gamma_0$. Meanwhile, at high temperatures (dashed), $T > T_1$, it is hard to see the signature of the topological phase transition between the gapped NTS and gapless TS_4 phases. We notice that as temperature increases, κ_T increases in the superfluid phase, while it decreases in the normal phase. Figures 5(c) and 5(d) are plots of both 2D and 3D chemical potentials as functions of Γ/Γ_0 for $T = 0.1E_F$ (solid) and $T = 0.45E_F$ (dashed), respectively. It shows that μ is an increasing function of T and μ in the superfluid phase is varying slowly compared with that in the normal phase. Even though the signatures of the topological transitions, which are strong at zero temperature, are weakened by the thermal fluctuations, the characteristic features for the variations of the thermodynamic quantities near the phase transitions remain the same.

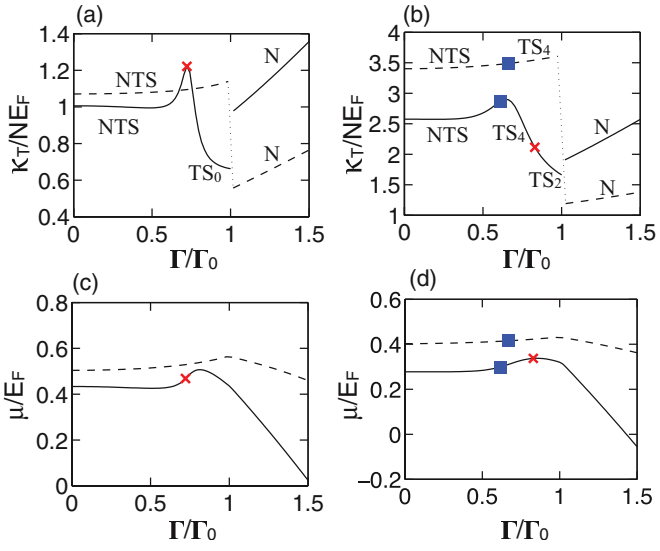

FIG. 5. (Color online) Isothermal compressibility κ_T and chemical potential μ as a function of Γ/Γ_c for (a),(c) 2D and (b),(d) 3D Fermi gas at temperature $T = 0.1E_F$ (solid) and $T = 0.45E_F$ (dashed). We indicates topological phase transitions with red cross (Γ_c) and blue squares (Γ_Δ) within the uniform superfluid phases. One finds that normals (N) to superfluid phase transitions occur at Γ_0 and are characterized by the discontinuity of the isothermal compressibility κ_T, while the chemical potential μ remains a continuous function of Γ as well as a function of T.

In Fig. 6, we present the other relevant thermodynamic quantities in 2D and 3D Fermi gases, such as pressure p, entropy S, and specific heat c_V, which can be observed experimentally, as a function of Γ/Γ_0 at $T = 0.1E_F$ (solid) and $T = 0.45E_F$ (dashed). We choose $E_b = 0.5E_F$ for 2D and

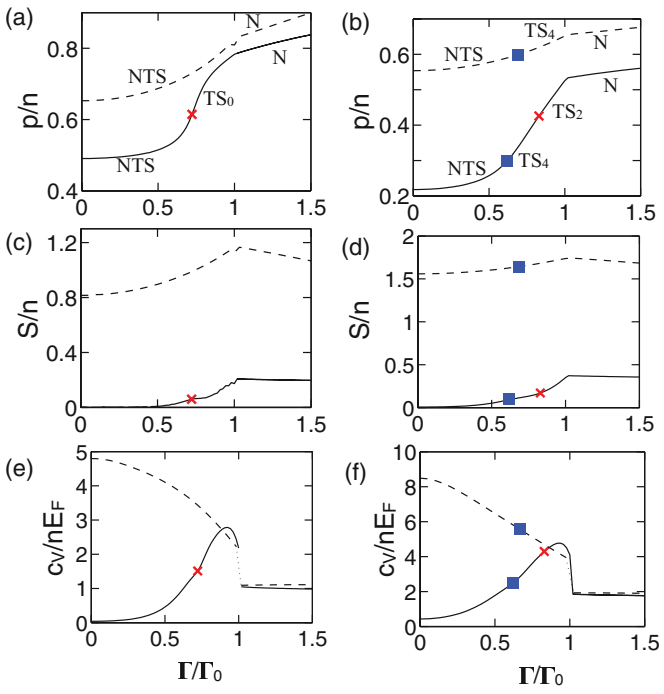

FIG. 6. (Color online) Pressure p, entropy S, and specific heat c_V as a function of Γ/Γ_0, where Γ_0 corresponds to the Zeeman field at $\Delta = 0$, for (a),(c),(d) 2D Fermi gas at $E_b = 0.5E_F$ and (b),(d),(f) 3D Fermi gas at $1/K_F a_s = 0$ at $T = 0.1E_F$ (solid) and $T = 0.45E_F$ (dashed). We used the red cross and blue square for Γ_c and Γ_Δ, respectively. One notices that the signatures of the normal (N) to superfluid phase transitions are visible in both 2D and 3D Fermi gases, characterized by the suppression of p and S in the superfluid state and the discontinuity of c_V. On the other hand, it is difficult to observe the topological phase transitions even with some weak signatures.

$1/K_F a_s = 0$ for 3D Fermi system with Rashba SOC $\alpha K_F = 0.4$. The main conclusion from these calculations is that the signatures of the topological phase transitions are much weaker in these quantities than those of ordinary phase transitions from the ordinary s-wave superfluid to normal phases.

V. CONCLUSIONS

In summary, we have investigated the two- and three-dimensional uniform fermion s-wave superfluids in the presence of Rashba spin-orbit coupling together with Zeeman field as they undergo topological phase transitions as a function of the interaction parameter ν and Zeeman field Γ at zero temperature and as a function of Zeeman field Γ at finite temperatures. In 2D s-wave Fermi gas, for $\Gamma = \Gamma_c = \sqrt{\mu^2 + \Delta^2}$ the superfluid phase is identified with a gapless topological superfluid (with one node at $k = 0$), while it becomes a fully gapped nontopological superfluid phase at $\Gamma < \Gamma_c$ and a fully gapped topological superfluid phase TS_0, capable of supporting Majorana fermion excitations at order parameter defects such as vortices, at $\Gamma > \Gamma_c$. The TS_0 phase has recently received wide attention in condensed matter physics [31–36,39–41] where 2D semiconducting thin films and 1D semiconducting nanowires with proximity induced s-wave superconductivity and a Zeeman field have been shown to support Majorana fermions in order parameter defects such as vortices and boundaries. Such localized Majorana fermion excitations are thought to support non-Abelian statistics, which has been proposed as a key resource for fault-tolerant topological quantum computation (TQC) [42]. In contrast, 3D s-wave Fermi gas is a fully gapped nontopological superfluid at $\Gamma < \Delta$, becomes a gapless topological superfluid with four topologically protected Weyl fermion points [37] at $\Delta < \Gamma < \Gamma_c$ and another topological superfluid with two topologically protected Weyl fermion points at $\Gamma > \Gamma_c$. With our calculated mean-field phase diagrams in both 2D and 3D we investigated the thermodynamic properties across the relevant topological phase transitions, including the isothermal compressibility, chemical potential, pressure, entropy, and specific heat as functions of the Zeeman field Γ and the interaction parameter ν. In particular, the isothermal compressibility of the system supporting the Majorana fermions, which is the 2D fermion gas with Rashba SOC together and a perpendicular Zeeman field, reveals the topological phase transition via a strong peak at the critical point $\Gamma = \Gamma_c$ (Fig. 3). Furthermore, the phase boundary can also be identified by the chemical potential through the change of the curvature as a function of Γ (Fig. 2). For the 3D Fermi gas, the topological phase transition from the fully gapped nontopological phase to the gapless topological phases can be probed by the position of the peak in the isothermal compressibility as a function of Γ, even if the signatures of the topological transitions are weaker than those in the 2D system. The signatures of the topological phase transitions at low temperature disappear as the temperature goes above the critical temperature T_1. The other thermodynamic quantities, such as pressure, entropy, and specific heat, have only weak signatures of the topological phase transitions [that is, the transition between a conventional (nontopological) superfluid and a topological superfluid such as the Majorana and the Weyl phases], while these are useful quantities to identify the phase transitions from the normal phase to the topological superfluid phases with decreasing values of the Zeeman field.

ACKNOWLEDGMENTS

K.S. is grateful to Carlos A. R. Sá de Melo for valuable discussions. This work is supported by AFOSR (FA9550-13-1-0045), DARPA MTO (FA9550-10-1-0497), NSF-PHY (1104546), and ARO (W911NF-12-1-0334).

[1] C. Chin, R. Grimm, P. Julienne, and E. Tiesinga, Rev. Mod. Phys. **82**, 1225 (2010).
[2] S. Giorgini, L. P. Pitaevskii, and S. Stringari, Rev. Mod. Phys. **80**, 1215 (2008).
[3] C. A. Regal, M. Greiner, and D. S. Jin, Phys. Rev. Lett. **92**, 040403 (2004); M. W. Zwierlein, C. A. Stan, C. H. Schunck, S. M. F. Raupach, A. J. Kerman, and W. Ketterle, *ibid.* **92**, 120403 (2004); M. Bartenstein, A. Altmeyer, S. Riedl, S. Jochim, C. Chin, J. H. Denschlag, and R. Grimm, *ibid.* **92**, 120401 (2004).
[4] J. T. Stewart, J. P. Gaebler, T. E. Drake, and D. S. Jin, Phys. Rev. Lett. **104**, 235301 (2010).
[5] M. W. Zwierlein, J. R. Abo-Shaeer, A. Schirotzek, C. H. Schunck, and W. Ketterle, Nature (London) **435**, 1047 (2005).
[6] M. W. Zwierlein, A. Schirotzek, C. H. Schunck, and W. Ketterle, Science **311**, 492 (2006).
[7] G. B. Partridge, W. Li, R. I. Kamar, Y. Liao, and R. G. Hulet, Science **311**, 503 (2006).
[8] Y. Liao *et al.*, Nature (London) **467**, 567 (2010).
[9] K. Martiyanov, V. Makhalov, and A. Turlapov, Phys. Rev. Lett. **105**, 030404 (2010).
[10] M. Feld, B. Fröhlich, E. Vogt, M. Koschorreck, and M. Köhl, Nature (London) **480**, 75 (2011).
[11] Y.-J. Lin, K. Jimenez-Garcia, and I. B. Spielman, Nature (London) **471**, 83 (2011).
[12] J.-Y. Zhang, S.-C. Ji, Z. Chen, L. Zhang, Z.-D. Du, B. Yan, G.-S. Pan, B. Zhao, Y.-J. Deng, H. Zhai, S. Chen, and J.-W. Pan, Phys. Rev. Lett. **109**, 115301 (2012).
[13] C. Qu, C. Hamner, M. Gong, C. Zhang, and P. Engels, arXiv:1301.0658.
[14] P. Wang, Z.-Q. Yu, Z. Fu, J. Miao, L. Huang, S. Chai, H. Zhai, and J. Zhang, Phys. Rev. Lett. **109**, 095301 (2012).
[15] L.W. Cheuk, A.T. Sommer, Z. Hadzibabic, T. Yefsah, W. S. Bakr, and M.W. Zwierlein, Phys. Rev. Lett. **109**, 095302 (2012).
[16] M. Chapman and C. Sá de Melo, Nature (London) **471**, 41 (2011); J. P. Vyasanakere, S. Zhang, and V. B. Shenoy, Phys. Rev. B **84**, 014512 (2011); Hui Hu, Lei Jiang, Xia-Ji Liu, and Han Pu, Phys. Rev. Lett. **107**, 195304 (2011); Z.-Q. Yu and H. Zhai, *ibid.* **107**, 195305 (2011); M. Iskin and A. L. Subasi, *ibid.* **107**, 050402 (2011); Gang Chen, Ming Gong, and Chuanwei Zhang, Phys. Rev. A **85**, 013601 (2012); L. Han and C. A. R. Sá de Melo, *ibid.* **85**, 011606(R) (2012); K. Seo,

L. Han, and C. A. R. Sá de Melo, *ibid.* **85**, 033601 (2012); L. Han and C. A. R. Sá de Melo, arXiv:1206.4984v1; Z. Zheng, M. Gong, X. Zhou, C. Zhang, and G.-C. Guo, Phys. Rev. A **87**, 031602(R) (2013).
[17] M. Gong, S. Tewari, and C. Zhang, Phys. Rev. Lett. **107**, 195303 (2011).
[18] M. Gong, G. Chen, S. Jia, and C. Zhang, Phys. Rev. Lett. **109**, 105302 (2012).
[19] K. Seo, L. Han, and C. A. R. Sá de Melo, Phys. Rev. Lett. **109**, 105303 (2012).
[20] Y. A. Bychkov and E. I. Rashba, J. Phys. C **17**, 6029 (1984).
[21] G. Dresselhaus, Phys. Rev. **100**, 580 (1955).
[22] Chuanwei Zhang, Sumanta Tewari, Roman M. Lutchyn, and S. Das Sarma, Phys. Rev. Lett. **101**, 160401 (2008).
[23] M. Sato, Y. Takahashi, and S. Fujimoto, Phys. Rev. Lett. **103**, 020401 (2009).
[24] P. B. Pal, Am. J. Phys. **79**, 485 (2011).
[25] N. Navon *et al.*, Science **328**, 729 (2010).
[26] M. J. H. Ku, A. T. Sommer, L. W. Cheuk, and M. W. Zwierlein, Science **335**, 563 (2012).
[27] N. Nagaosa, J. Sinova, S. Onoda, A. H. MacDonald, and N. P. Ong, Rev. Mod. Phys. **82**, 1539 (2010).
[28] D. Xiao, M.-C. Chang, and Q. Niu, Rev. Mod. Phys. **82**, 1959 (2010).
[29] M. Z. Hasan and C. L. Kane, Rev. Mod. Phys. **82**, 3045 (2010).
[30] X.-L. Qi and S.-C. Zhang, Rev. Mod. Phys. **83**, 1057 (2011).
[31] J. D. Sau, R. M. Lutchyn, S. Tewari, and S. Das Sarma, Phys. Rev. Lett. **104**, 040502 (2010).
[32] J. D. Sau, S. Tewari, R. M. Lutchyn, T. Stanescu,and S. Das Sarma, Phys. Rev. B **82**, 214509 (2010).
[33] R. M. Lutchyn, J. D. Sau, and S. Das Sarma, Phys. Rev. Lett. **105**, 077001 (2010).
[34] Y. Oreg, G. Refael, and F. von Oppen, Phys. Rev. Lett. **105**, 177002 (2010).
[35] L. Mao, J. Shi, Q. Niu, and C. Zhang, Phys. Rev. Lett. **106**, 157003 (2011).
[36] L. Mao, M. Gong, E. Dumitrescu, S. Tewari, and C. Zhang, Phys. Rev. Lett. **108**, 177001 (2012).
[37] G. E. Volovik, *The Universe in Helium Droplet* (Clarendon, Oxford, 2003).
[38] J. D. Sau and S. Tewari, Phys. Rev. B **86**, 104509 (2012).
[39] V. Mourik, K. Zuo, S. M. Frolov, S. R. Plissard, E. P. A. M. Bakkers, and L. P. Kouwenhoven, Science **336**, 1003 (2012).
[40] M. T. Deng, C. L. Yu, G. Y. Huang, M. Larsson, P. Caroff, and H. Q. Xu, Nano Lett. **12**, 6414 (2012).
[41] A. Das, Y. Ronen, Y. Most, Y. Oreg, M. Heiblum, and H. Shtrikman, Nat. Phys. **8**, 887 (2012).
[42] C. Nayak, S. H. Simon, A. Stern, M. Freedman, and S. Das Sarma, Rev. Mod. Phys. **80**, 1083 (2008).